Deng, M.; Wang, L.; Höche, D.; Lamaka, S.; Snihirova, D.;
Vaghefinazari, B.; Zheludkevich, M.:

Clarifying the decisive factors for utilization efficiency of Mg anodes for primary aqueous batteries.

In: Journal of Power Sources. Vol. 441 (2019) 227201.
First published online by Elsevier: 17.10.2019

https://dx.doi.org/10.1016/j.jpowsour.2019.227201

Clarifying the decisive factors for utilization efficiency of Mg anodes for primary aqueous batteries

Min Deng[a,*], Linqian Wang[a], Daniel Höche[a, b], Sviatlana V. Lamaka[a], Darya Snihirova[a], Bahram Vaghefinazari[a], Mikhail L. Zheludkevich [a, c]

[a] MagIC – Magnesium Innovation Centre, Helmholtz-Zentrum Geesthacht (HZG), 21502 Geesthacht, Germany

[b] Computational Material Design, Faculty of Mechanical Engineering, Helmut-Schmidt-University University of the Federal Armed Forces, 22043 Hamburg, Germany

[c] Institute of Materials Science, Faculty of Engineering, Kiel University, 24143 Kiel, Germany

Abstract: Low anodic efficiency of metallic Mg, which results in low discharge capacity and specific energy density, hinders the wider application of aqueous primary Mg batteries. In this work, we clarify the decisive factors effecting the utilization efficiency of Mg anodes. Anodic efficiency of several Mg anodes at different current densities is measured in 3.5 wt.% NaCl electrolyte. The contribution of self-corrosion at open circuit potential and at constant applied current to efficiency of Mg anodes is compared. Additionally, efficiency loss caused by detachment of undissolved metallic portions, namely "chunk effect", is determined with a proposed new approach. The effect of self-corrosion and "chunk effect" on anodic efficiency is assessed accordingly. The results indicate that "chunk effect" can also result in large efficiency loss of Mg anodes, especially at low current densities, which, in some cases, could exceed the loss caused by other mechanisms of self-corrosion of anode substrate. Hence, attention should be paid to both aspects when developing novel Mg anodes with high anodic efficiency, particularly for application in long-term low-power battery system.

Key words: Mg batteries; Anodic efficiency; Self-corrosion; Chunk effect.

* Corresponding author.
E-mail address: Min.Deng@hzg.de (M. Deng), Telephone number: +49 (0)4152 871936, Postal address: Helmholtz-Zentrum Geesthacht, Max-Planck-Str. 1, 21502 Geesthacht, Germany.

1. Introduction

Nowadays, the wide application and commercialization of primary aqueous Mg batteries are still hindered in spite of the attractive theoretical properties of these promising energy storage devices. The issues could be partially originated from the cathode materials, such as the sluggish kinetics of cathodic reactions or the limited diffusion of reactants, leading to large overvoltage. The problems concerning cathode materials have been widely discussed in the last decades [1-4] and some approaches have been proposed as effective solutions, like the adoption of selected advanced catalysts and porous substrate materials with nanostructures [5-10]. However, there are also major issues relevant to the Mg anode materials, including large overpotential caused by discharge products on anode surface and severe self-corrosion of Mg under polarization due to the well-known NDE [11-13]. These problems still exist despite recent progresses achieved through the development of novel Mg alloy anodes [14-17] and electrolyte additives [18-22]. Therefore, more effort needs to be made for modification and optimization of Mg anodes.

The anodic efficiency (or utilization efficiency) has great impact on the specific performance of aqueous Mg-based battery system, e.g., energy density and service life. The decreased anodic efficiency leads to low discharge capacity and specific energy density of Mg batteries, since a large portion of Mg anode is consumed via self-corrosion processes and, consequently, does not participate in the power supply. Unfortunately, the utilization efficiency of Mg anodes is normally below 60% at current density of 10 mA cm^{-2} and was found to be even less than 50% under smaller current densities [15, 23-29]. As a consequence, the reported optimized specific energy density, like 1800 Wh kg^{-1} in Mg-air system [14], is far below the theoretical level (6800 Wh kg^{-1} based on anode only). Hence, the service life of primary Mg-based batteries are severely shortened, especially for those battery system designed for long-term and low power applications. Generally, the utilization efficiency of Mg anodes is inversely proportional to the weight loss caused by self-corrosion during discharge. In fact, the self-corrosion of Mg includes two different processes, namely the

electrochemical dissolution of Mg substrate and the detachment of some metallic pieces from anode surface, which is known as “chunk effect” (CE). CE has been shown in some publications at the cross section morphology of Mg after corrosion tests. It is identified by the existence of some metallic pieces in corrosion products, including impurity particles, second phases or undissolved matrix [14, 30-33].

Until now, nearly all the published work regarding improving the utilization efficiency of Mg anodes follows the direction of controlling the self-corrosion of anode substrate. Meanwhile, the corrosion resistance measured via electrochemical impedance spectroscopy (EIS) and corrosion rate determined with hydrogen evolution (HE) at open circuit potential (OCP) are normally utilized to conclude the effect of self-corrosion on Mg anode efficiency at different current densities. However, the feasibility of evaluating the real time self-corrosion rate of Mg during discharge based on determined corrosion behavior at OCP is doubtful. To the best of our knowledge, no published research has put emphasis on particularly clarifying this issue. Nonetheless, relevant information can be found from some publications. In the published paper of Samaniego et al. [34], Mg-33.at%Li alloy exhibits lower HE rate than pure Mg at OCP, but its HE rate becomes similar or even higher than pure Mg with applied anodic current densities. Similarly, according to the work of Chu et al. [35], HE rate of Mg-Zn-Ca-Mn alloy is similar to pure Mg in NaCl solution with applied current density of 1 mA cm^{-2} but tends to be higher when the current density increases to 10 mA cm^{-2}. Therefore, more systematic work is necessary to specify the relevance of self-corrosion to anodic efficiency of different Mg alloy anodes, especially under varying current densities. On the other hand, the impact of CE on anode utilization efficiency seems to be not fully taken into account in the selection procedure of Mg alloy anodes [15-17, 20, 23, 27, 29, 36-41]. Only a few published works mention the possible influence of CE when evaluating the anodic efficiency of Mg anodes [14, 28, 42-44]. In fact, opposite results regarding utilization efficiency of same Mg anodes are found at different current densities in the work of Wang et al [28]. Mg-Al-Pb-In anode has lower utilization

efficiency than Mg-Al-Pb and pure Mg anode at current density of 10 mA cm^{-2}. However, adverse results are obtained when the current density increases to 180 and 300 mA cm^{-2}, as Mg-Al-Pb-In anode exhibits the highest efficiency comparing to the other two anode materials. The inconsistent utilization efficiency is supposed to be the consequence of different extent of CE at different current densities, concluded from the different surface morphologies after discharge. Despite the absence of more direct evidence in that work, it demonstrates that CE could have decisive effect on the utilization efficiency of Mg anodes.

In this present work, we examine the influence of the decisive factors for anodic efficiency of Mg anodes in aqueous electrolyte under relatively small load. Corrosion resistance and self-corrosion rate at OCP of high purity Mg (HP Mg) and several industrially relevant Mg alloys are determined through EIS and HE tests as well as the real time HE rate during discharge at different current densities. The possible occurrence of CE on these anode materials is observed from the cross section morphology after discharge tests. Meanwhile, the anodic efficiency of these selected Mg anodes after discharge are measured. The efficiency loss resulted from self-corrosion of anode substrate and CE is determined respectively by a proposed approach. Accordingly, the effect of both self-corrosion and CE on anodic efficiency of Mg anodes is evaluated.

2. Experimental procedures

Six magnesium alloys were used in this work. Of these, the discharge properties of HP Mg, AZ31 and AM50 alloys as anode for Mg-air batteries have been reported in our previous work [14]. Besides, we also investigated three more industrially relevant Mg alloys with different chemical compositions, i.e., Elektron 21 (E21 hereafter), WE43 and ZE41, which are the same materials studied in the published work of Lamaka et al., where new corrosion inhibitors for Mg were reported [22]. All six possess significantly different corrosion rates. All the samples were taken from as-cast ingots of corresponding materials. The chemical composition of all studied materials is presented in

Table 1, showing the contents of all main elements and detrimental impurities like Fe, Cu and Ni. Fig. S1 in the supplementary materials shows the micrographs of all materials after polishing via a Tescan VEGA scanning electron microscope (SEM), indicating different microstructures, including diverse second phase fraction and distribution.

Table 1 Chemical composition of as-cast HP Mg and Mg alloys [14, 22]. The values are in ppm if other is not indicated.

Element	HP Mg	AZ31	AM50	E21	WE43	ZE41
Fe	50	11	2	12	38	18
Cu	<1	19	17	20	47	19
Ni	<2	7	5	52	46	7
Si	<1	309	637	4	0.9	2
Ca	<1	11	11	42	225	27
Zn	35	0.73%	418	0.29%	268	4.2%
Mn	8	0.36%	0.43%	38	60	79
Al	30	2.97%	4.85%	145	133	144
Zr	-	-	-	0.19%	0.17%	0.3%
Nd	-	-	-	3.2%	1.95%	0.24%
La	-	-	-	26	0.14%	0.42%
Pr	-	-	-	340	0.1%	647
Th	-	-	-	920	0.15%	0.29%
Y	-	-	-	72	4.49%	50
Ce	-	-	-	70	206	0.65%
Mg	99.98%	95.90%	94.61%	96.09%	92.85%	93.75%

HE rate on different Mg anodes at open circuit potential was determined with an ordinary set-up, which includes a funnel inserted into a 100 ml inverted burette (0.2ml graduations) and covering the sample. The specimens, with surface area of approximately 8 cm^2, were hung up with fishing line via an inserted plastic screw. The solution for all the measurements in this work was 3.5 wt.% NaCl unbuffered solution prepared with deionized water, with pH of around 5.6. Before immersion, all the

specimens were ground with SiC sand paper up to 1200 grit. The immersion test for each material was repeated three times to ensure the reproducibility. The duration time of each immersion measurement was 100 hours.

Real-time HE rate during discharge was measured with a similar set-up used in the work of Frankel et al. [45] to collect the gas during galvanostatic polarization of Mg. The schematic corresponding to this experimental set-up is presented in Fig. S2. A Gamry Potentiostat was used to apply current to the Mg anodes in galvanostatic mode. A classical three-electrode system was adopted with Mg samples embedded into epoxy as a working electrode, exposing one rectangle surface with 1 cm^2. The counter electrode and reference was Pt wire and saturated Ag/AgCl electrode, respectively. Evolved hydrogen was collected via the 50 ml inverted burette with graduations of 0.1 ml. The volume of evolved hydrogen was determined under applied current densities of 1 mA cm^{-2}, 5 mA cm^{-2} and 10 mA cm^{-2}. The duration time for 1 mA cm^{-2} was 6 hours, while for 5 and 10 mA cm^{-2} is 90 and 60 minutes respectively due to the rapid hydrogen evolution rate under severe polarization. Real-time HE rate was then calculated according to the recorded data. Note that only data in the later discharge period was used for calculation after a relatively constant HE rate was achieved. In detail, HE data after 3 hours was used for 1 mA cm^{-2}, while data after 30 minutes was used for 5 and 10 mA cm^{-2}. Real-time HE measurement was carried out twice, showing a low deviation below 10%.

Electrochemical impedance was also measured to evaluate the corrosion resistance of different Mg anodes. Each sample was carefully treated with sand paper and then immersed into the solution with 1 cm^2 working surface. EIS measurements were performed after one-hour OCP test in order to obtain relatively stable surface condition. The scanned frequency ranged from 100 kHz to 0.01 Hz with sinusoidal excitation voltage of 10 mV rms referred to OCP.

Half-cell discharge test at different current densities was carried out in 3.5 wt.% NaCl electrolyte. The discharge process under 1 mA cm^{-2} lasts 16 hours, while 8 hours in the case of 5 mA cm^{-2} and

10 mA cm^{-2}. After discharge, precipitated products were removed from the surface with chromic acid (200 g L^{-1} CrO_3) and the anode utilization efficiency of each material was calculated. . The details of the calculation procedure can be found elsewhere [14, 46]. The surface morphology after discharge and cleaning the discharge products was observed with SEM. The morphology of corresponding cross section for each anode after discharge at 5 mA cm^{-2} for 16 hours was also observed. Additionally, elemental mapping for selected zones in cross section was determined with the SEM coupled with energy dispersive X-ray spectroscopy (EDS) via backscattered-electrons (BSE) detector at 15 kV.

3. Results and discussion

3.1 Anodic efficiency during discharge

Fig. 1 presents the discharge curves and anodic efficiency of pure Mg and different Mg alloys. During the 15-hours discharge measurement, all the materials maintain relatively stable discharge potential after the initial unstable periods for approximately one hour. This indicates that all the Mg anodes can keep a steady surface condition during the long-term discharge, attributed to the balance between actual surface area, changing pH, accumulation and self-peeling of discharge products. The discharge potential is relevant to the Mg anode composition, which, however, is not the emphasis of this work. According to Fig. 1(b), these six Mg anodes show rather different anodic efficiency after discharge at various current densities. HP Mg exhibits highest anodic efficiency at all current densities, with that being above 50% at 5 and 10 mA cm^{-2}. Anodic efficiency of AZ31 alloy approaches that of HP Mg at 5 and 10 mA cm^{-2}. E21 alloy shows second highest anodic efficiency at 1 mA cm^{-2}, but with increasing current density its anodic efficiency becomes inferior comparing to HP Mg, AZ31 as well as WE43, which shows lower efficiency than E21 anode at 1 and 5 mA cm^{-2}. AM50 alloy has lower efficiency than E21 alloy at different current densities. However, the difference tends to be less with increasing current densities from 1 to 10 mA cm^{-2}. Among all the

measured materials, ZE41 alloy possesses the lowest anodic efficiency at all current densities. It is worth noting that nearly all the anodes show enhanced anodic efficiency at higher discharge current density, except E21 and ZE41 at current density of 5 mA cm^{-2}. As mentioned in the introduction section, the anodic efficiency of Mg anodes depends on the self-corrosion performance, including substrate dissolution rate and the CE. The respective contribution of substrate dissolution rate and CE on efficiency loss may vary with different current densities, leading to the different anodic efficiency of Mg anodes at each current density. Therefore, we would like to investigate the effect from both aspects, respectively, in the following sections.

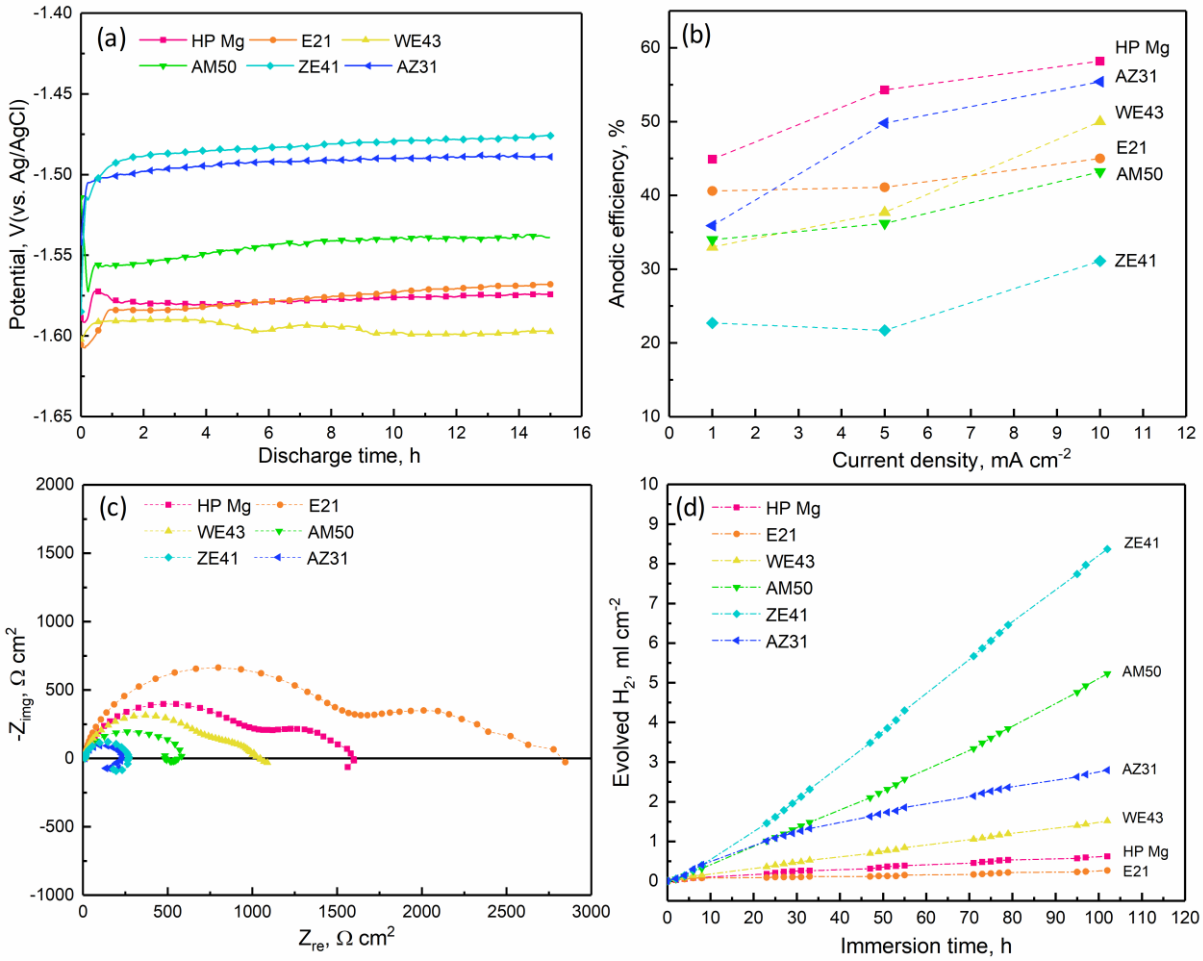

Fig. 1. (a) Discharge curves of high purity Mg and Mg alloys at 5 mA cm^{-2}; (b) Anodic efficiency after discharge at different current densities; (c) EIS (Nyquist plots) at OCP; (d) Hydrogen evolution curves of all selected materials. All the measurements are performed in unbuffered 3.5 wt.% NaCl solution.

3.2 Self-corrosion rate

3.2.1 Self-corrosion at OCP

EIS and hydrogen evolution test are commonly used to evaluate the corrosion resistance and corrosion rate of magnesium [12]. Fig. 1(c) presents the results of EIS measurement for all selected materials at OCP after immersion for one hour in 3.5 wt.% NaCl solution. Obviously, these materials have completely different impedance, indicating varying corrosion resistance following the order: E21 > HP Mg > WE43 > AM50 > ZE41 > AZ31. Nevertheless, these results can only reflect the initial corrosion resistance of these materials. Mg alloys with different chemical composition typically show different corrosion behavior after long immersion time due to the changing surface condition, such as the formation of protective oxide film [47-49]. The hydrogen evolution curves obtained from immersion test in 3.5 wt.% NaCl solution for more than 100 hours are indicated in Fig. 1(d) and utilized to evaluate the overall self-corrosion rate of these Mg anodes. The average self-corrosion rate calculated from hydrogen evolution test are presented in Table 2, following the order: E21 < HP Mg < WE43 < AZ31 < AM50 < ZE41. For all the materials, the results obtained from hydrogen evolution test are consistent with the EIS results except AZ31 alloy. It is not surprising because from the hydrogen evolution curves we can see that, during the initial stage of immersion (see Fig. S3), AZ31 alloy shows the fastest hydrogen evolution rate, indicating the highest self-corrosion rate, which is consistent with the EIS results. After immersion for nearly 30 hours, the hydrogen evolution rate of AZ31 decreases and becomes slower than that of AM50 and ZE41 alloys. Interestingly, from the comparison of anodic efficiency and self-corrosion rate of these Mg anodes, something noteworthy is that the self-corrosion rate at OCP of Mg anodes should not be used as a direct indicator for the utilization efficiency. For instance, E21 shows the lowest self-corrosion rate obtained from both EIS and hydrogen evolution test, but it has lower anodic efficiency than HP Mg and AZ31 alloys, especially at high current densities. AZ31 alloy exhibits higher efficiency than E21 and WE43 alloys, even though its hydrogen evolution rate at OCP (0.033 ml cm^{-2} h^{-1}) is greatly

higher than E21 (0.003 ml cm^{-2} h^{-1}) and WE43 (0.016 ml cm^{-2} h^{-1}). The hydrogen evolution rate of AM50 is 0.052 ml cm^{-2} h^{-1}, which is nearly 20 times that of E21. However, their utilization efficiencies at 10 mA cm^{-2}, which are 43.2% and 45% respectively, indicate little difference.

Table 2 Hydrogen evolution rate of high purity Mg and selected Mg alloys at OCP and under applied current in 3.5 wt.% NaCl solution.

Self- corrosion P_H (ml cm^{-2} h^{-1})	HP Mg	E21	WE43	AM50	ZE41	AZ31
OCP	$(6\pm2)\cdot10^{-3}$	$(3\pm1)\cdot10^{-3}$	$(16\pm1)\cdot10^{-3}$	$(52\pm3)\cdot10^{-3}$	$(87\pm15)\cdot10^{-3}$	$(33\pm7)\cdot10^{-3}$
1 mA cm^{-2}	0.3	0.4	0.3	0.6	0.8	0.5
5 mA cm^{-2}	1.6	1.6	1.7	1.8	3.0	1.7
10 mA cm^{-2}	3.0	3.8	3.1	3.0	6.0	3.2

3.2.2 Self-corrosion during discharge

In Fig. 2, the hydrogen evolution was recorded while applying different current densities so that the self-corrosion rate of Mg anodes during discharge can be compared. After an initial incubation period, all the materials maintained a relatively stable hydrogen evolution rate under different current densities. This incubation period lasts from several hours at low current density to less than 30 minutes at high current densities. Therefore, the real-time HE rate of these anode materials are calculated via the recorded HE data in the later discharge period with a relatively constant hydrogen evolution rate (more details in the section of experimental procedures). Table 2 shows the average value of hydrogen evolution rate obtained from two measurements that show deviation below 10%. No doubt that the hydrogen evolution rate of all the Mg anodes increases with increasing discharge current densities, which is a typical manifestation of the negative difference effect (NDE) of Mg in the unbuffered pH neutral NaCl solution. Interestingly, several alloys show similar hydrogen evolution rate measured with applied current, even though their self-corrosion rates at OCP appear to be of different magnitudes. At current density of 1 mA cm^{-2}, HP Mg and WE43 show the same

hydrogen evolution rate, which is even lower than E21 despite that their self-corrosion rates at OCP are higher than that of E21. At 5 mA cm^{-2}, the hydrogen evolution rates of all Mg anodes, but ZE41, indicate no large difference. The situation changes at 10 mA cm^{-2}, as the difference between the hydrogen evolution rates of these Mg anodes tends to be more distinct. Surprisingly, E21 alloy exhibits the second highest hydrogen evolution rate among all the studied materials while HP Mg and AM50 shows the lowest, which is completely inconsistent with their self-corrosion rates determined at OCP, Fig. 1d.

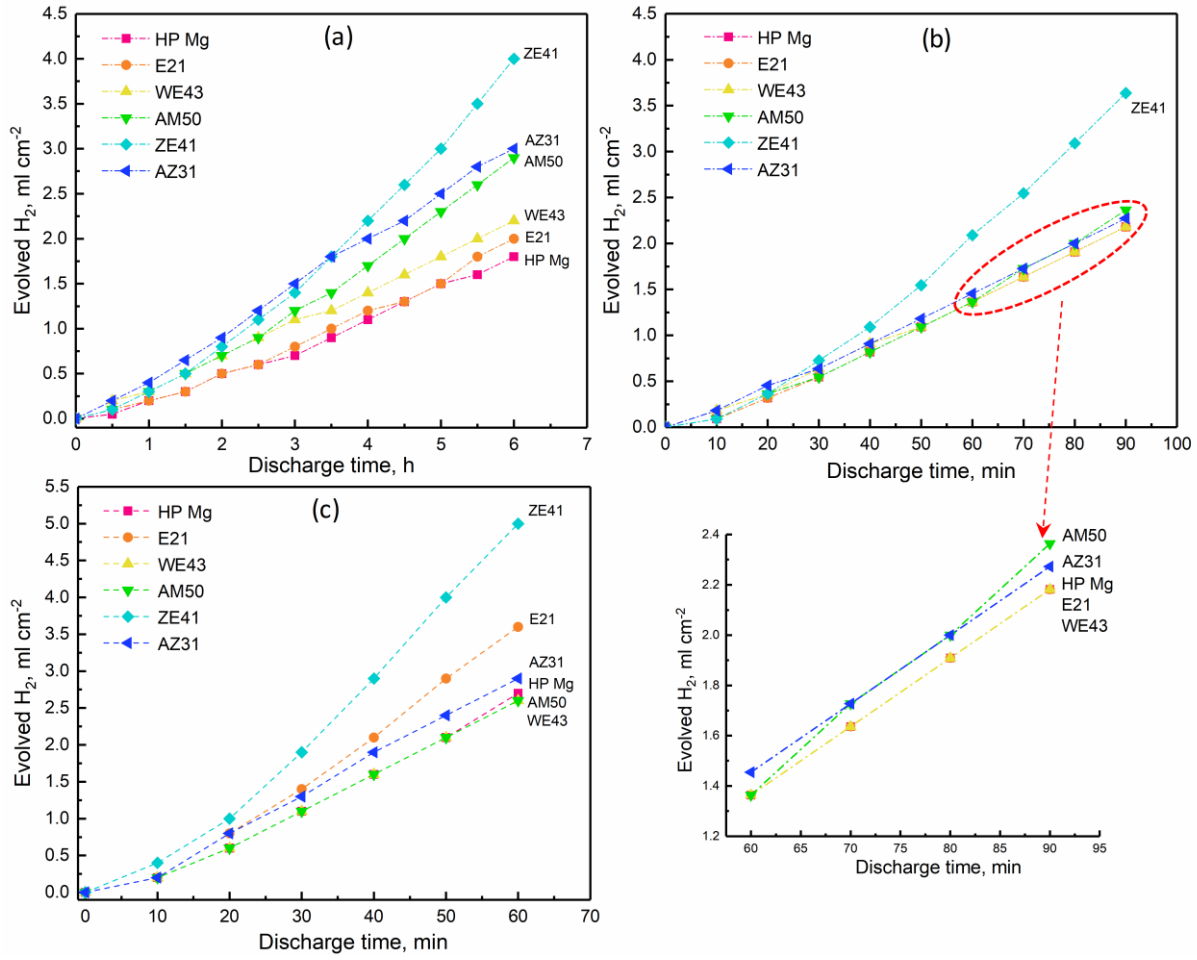

Fig. 2. Hydrogen evolution curves of different Mg anodes during discharge in 3.5 wt.% NaCl solution applied with different current densities: (a) 1 mA cm^{-2}; (b) 5 mA cm^{-2}; (c) 10 mA cm^{-2}. Typical results from replicated experiments are presented.

The plots of the hydrogen evolution rates of all selected Mg anodes as a function of applied current density are presented in Fig. 3. Within the current range in this work, from 1 mA cm^{-2} to 10

mA cm^{-2}, the hydrogen evolution rate of every material indicates a linearly increasing tendency with increasing current density. Previous reports show the examples of the linearly increasing hydrogen evolution rate for ultra-high purity Mg and AZ91 alloy in a wide range of current density [11, 45, 50, 51]. Fig. 3 also presents the linear fitting curves for all Mg anodes and lists the corresponding slope *k*, which represents the increase of hydrogen evolution rate as the function of current density. HP Mg, WE43, and AZ31 show similar slope, nearly 0.31, indicating a similar increasing tendency of hydrogen producing. By contrast, E21 and ZE41 exhibit much higher slopes than most materials, i.e., 0.38 and 0.58 respectively. This could be a sensible reason for the higher hydrogen evolution rate of E21 and ZE41 compared with other materials at high current density. The coefficient *k* for different Mg anode is probably dependent on the chemical composition and microstructure, which is beyond the scope of this work. In conclusion, the self-corrosion rate of Mg anodes during discharge varies with different current density and the corresponding increasing rate highly depends on the properties of the alloy.

Severe self-corrosion of Mg anodes during discharge, appearing as fast hydrogen evolution, is the most well-known reason for the large efficiency loss of Mg anodes in aqueous battery. Taking consideration of the real-time self-corrosion rate during discharge, we find it reasonable that HP Mg has the highest anodic efficiency among tested alloys due to its lowest self-corrosion rate under different current densities. Similarly, the highest self-corrosion rate of ZE41 anode during discharge could be an important reason for its lowest anodic efficiency. However, the anodic utilization efficiency of WE43 alloy could not be explained from the aspect of self-corrosion as it shows similar hydrogen evolution rate with HP Mg but inferior efficiency, which is even worse than AZ31 and E21, especially at low current densities. Note that, comparing to E21, the efficiencies of WE43 and AM50 anodes are much lower at low current densities but in similar level at high current density. This could be attributed to their varied hydrogen evolution rates under different current densities. E21 shows much higher hydrogen evolution rate than WE43 and AM50 at 10 mA cm^{-2} while reverse situation

happens with current density of 1 and 5 mA cm^{-2}. Regarding AZ31 alloy, its good anodic efficiency at all current densities seems to be contradictory with its relatively high self-corrosion rate during discharge. Therefore, it is sensible to pay more attention to the aforementioned "chunk effect" factor.

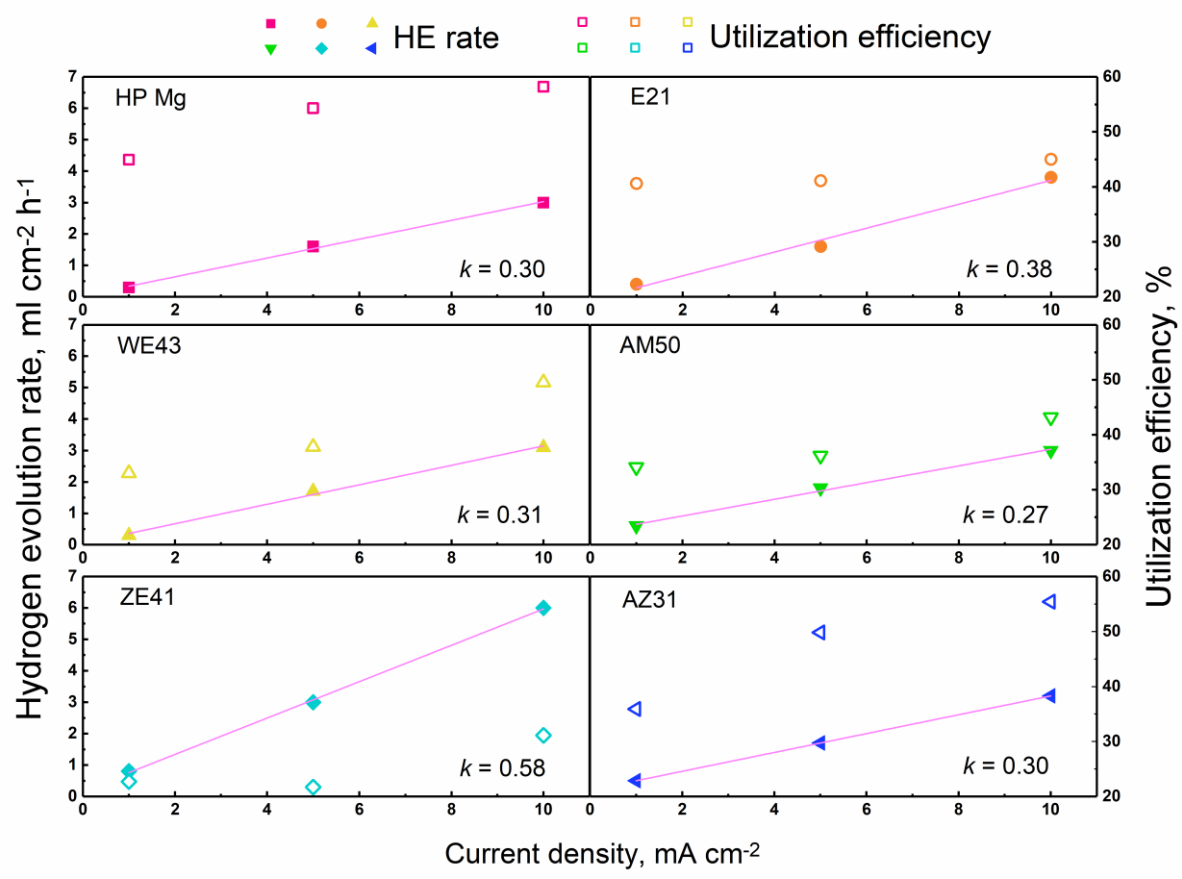

Fig. 3. Real-time hydrogen evolution rate as a function of applied current density. The solid symbols represent the measured real-time hydrogen evolution rate at different current densities. The straight lines are the linear fits with a slope of *k*. Utilization efficiency of all anodes is also presented for comparison as indicated by open symbols.

3.3 Influence of "chunk effect"

The efficiency loss resulting from CE cannot be directly determined by weight loss measurements since the undissolved anode parts will drop into the electrolyte and then degrade via independent self-corrosion processes. Other undissolved portions existing in the discharge products layer would fall out into the chromic acid solution in the chemical cleaning procedure. Therefore, we propose a novel method to calculate the efficiency loss caused by CE.

Generally, the specific weight loss (W) of Mg anode during discharge process can be expressed as following:

$$W = W_{discharge} + W_{self-corrosion} + W_{CE} \quad (1)$$

Where $W_{discharge}$ represents the weight loss resulting from Faradic process driven by the applied current, $W_{self\text{-}corrosion}$ means the weight loss caused by the self-corrosion of anode substrate and W_{CE} indicates the weight loss due to the mechanically detachment of undissolved anode portions. Therefore, similar to the equation for anode efficiency calculation [14, 46], anodic efficiency ($\boldsymbol{\eta}$) during discharge can also be defined as:

$$\eta = \frac{W_{discharge}}{W} \times 100\% \quad (2)$$

Meanwhile, the efficiency loss due to self-dissolution of anode substrate ($\boldsymbol{\eta}_{sc}$) is defined as:

$$\eta_{sc} = \frac{W_{self-corrosion}}{W} \times 100\% \quad (3)$$

Hence, the efficiency loss caused by CE ($\boldsymbol{\eta}_{ce}$) can be calculated via the following relationship:

$$\eta_{ce} = \frac{W_{Chunk\ effect}}{W} \times 100\% = 100\% - \eta - \eta_{sc} \quad (4)$$

The anodic efficiency $\boldsymbol{\eta}$ is determined after removing the discharge products from anode surface and presented in Fig. 1(d). In this context, $\boldsymbol{\eta}_{ce}$ can also be obtained supposing that the efficiency loss due to self-corrosion ($\boldsymbol{\eta}_{sc}$) were known. Meanwhile, the weight loss due to self-corrosion of Mg is directly proportional to the volume of produced hydrogen gas (assuming that water reduction accompanied by hydrogen evolution is by far the main cathodic reaction during Mg corrosion at anodic polarizations and the contribution of oxygen reduction is negligible [52]). Hence, it could be possible to determine the weight loss caused by self-corrosion and corresponding $\boldsymbol{\eta}_{sc}$ via the measured hydrogen evolution data if the collected hydrogen were all produced by self-corrosion of Mg substrate. However, it should be noted that the detached undissolved anode parts (chunks) also

produce hydrogen gas during corrosion, which definitely affects the determination. Therefore, to minimize the contribution of the chunk effect into the self-corrosion quantified by measuring H_2 evolution, the hydrogen evolution tests with applied current are only performed for relatively short time after a constant hydrogen evolution rate appears. The applied measurement durations are decided according to the time for the initial formation of CE, which is estimated from the cross section morphologies of WE43 and ZE41 alloys after discharge for different time (as shown in Fig. 4). After discharge at 1 mA cm^{-2} for 4 hours, both WE43 and ZE41 do not show apparent "chunks" in the discharge products. When the discharge time increases to 6 hours, the formation of "chunk" does not happen on WE43. In contrast, visible "chunks" are found from ZE41 alloy. At 10 mA cm^{-2}, CE is evident for both WE43 and ZE41 after discharge for 90 minutes. However, after discharge for 60 minutes, "chunks" are discovered only at cross section of ZE41 but not in the case of WE43. Note that, among all the studied Mg anodes, ZE41 offers the theoretically optimum condition for the formation of CE, attributed to the large fraction and continued distribution of second phases (see Fig. S1). Therefore, the selected time for real-time hydrogen evolution test at 1 mA cm^{-2} is 6 hours, while for 5 and 10 mA cm^{-2} the measurement time is only 90 and 60 minutes, respectively, as stated in the section of experimental procedures. It is reasonable to assume that, in these initial discharge periods, the produced hydrogen is mostly resulted from the dissolution of bulk anode substrate. Besides, we can know directly from Table 2 that the dissolution of Mg anode without applied current is dozens of times lower than its NDE-increased self-corrosion during discharge, especially at high current densities. It could be another evidence for the negligible effect of possible hydrogen evolution by "chunks" in the determination of η_{sc}. Another considerable factor is the stability of Mg hydrogen evolution rate during long-time discharge, in view of the varying anode surface and solution properties, like the composition and pH. On one hand, as discussed in section 3.1, generally all Mg anodes maintain a relatively steady surface condition during the long-term discharge, after initial stabilization period of one to two hours. Therefore, the issue concerning possibly changing surface

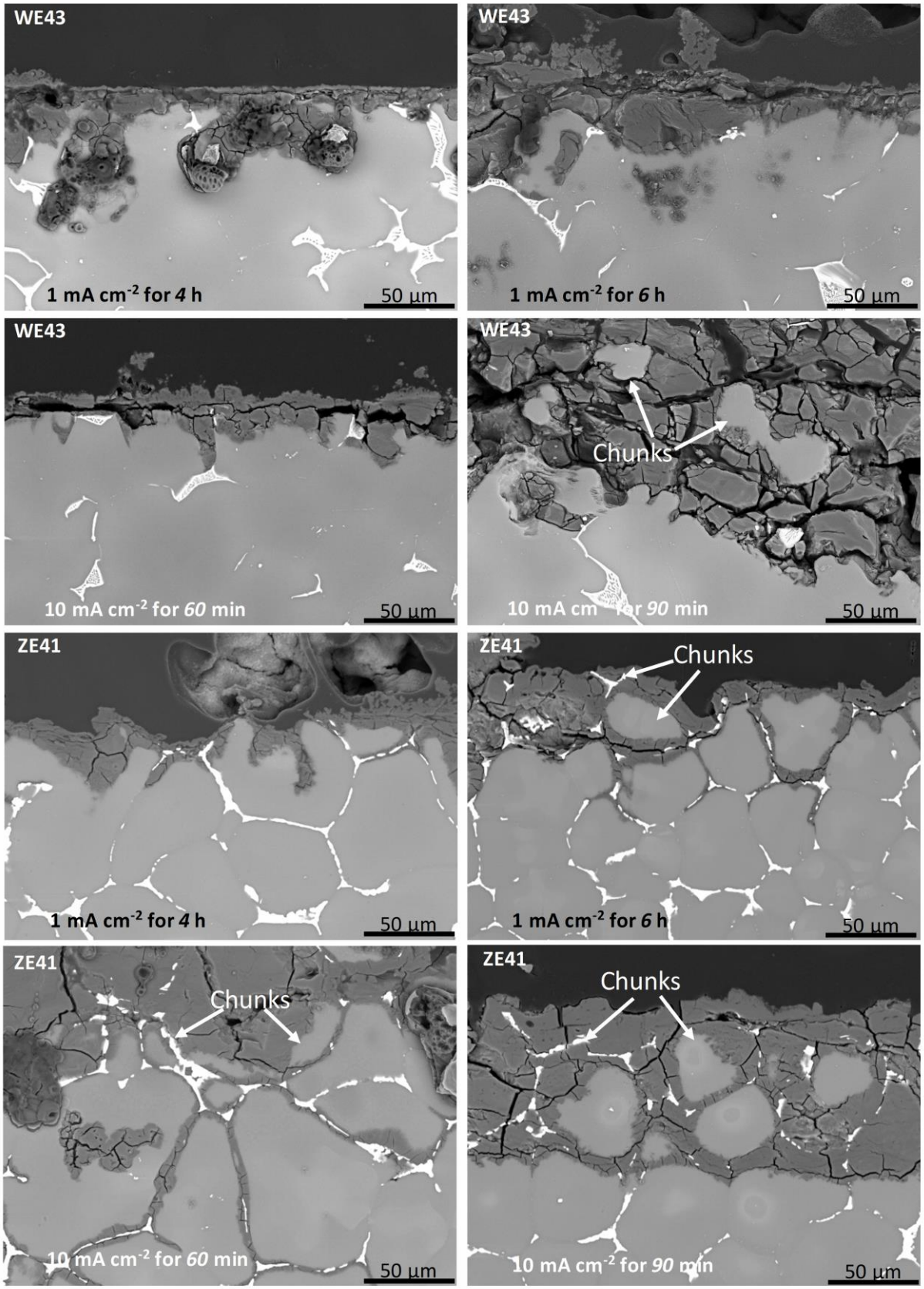

Fig. 4. Cross section morphologies of WE43 and ZE41 alloy after discharge for different duration time at 1 and 10 mA cm^{-2} in 3.5 wt.% NaCl solution.

condition can be ignored after the surface stabilization. On the other hand, possible influence of changing solution composition was clarified experimentally. The hydrogen evolution results during discharge of AM50 in fresh 3.5 wt.% NaCl solution and in similar solution remained in the electrochemical cell from previous experiment are presented in Fig. S4. The used solution is collected after a 15-hours discharge measurement at 5 mA cm^{-2} with AM 50 anode (1 cm^2 working surface). Note that this used solution was saturated with dissolved hydrogen, its pH was 10.8 and concentration of dissolved Mg^{2+} was 2.35 mM as shown by atomic absorption spectroscopy measurements. The results indicate that AM50 anode showed identical hydrogen evolution rate, 1.8 ml cm^{-2} h^{-1}, in fresh and in used electrolyte. The difference between the total volumes of evolved hydrogen gas originates from the initial stage of several minutes, which could be attributed to the solubility of hydrogen in water, fast increase of local and bulk pH, saturation with Mg^{2+} and other aspects. The results demonstrate that the changing solution composition and bulk pH during the discharge process have no apparent influence on the constant hydrogen evolution rate of AM50 (and possibly all other studied Mg anodes in this paper) at our experimental condition. This is also in agreement with previous reports were the fast increase of local pH near Mg surface after exposure in different media has been shown [53-55]. The rapid dissolution of Mg induced by applied current certainly accelerates the alkalization in the vicinity of Mg anodes, minimizing the effect of increasing bulk pH on self-corrosion. Therefore, eliminating the possible influence of these factors, the determined hydrogen evolution rate in the present work can be used to evaluate the self-corrosion rate of anodes during long-term discharge. Consequently, the proposed approach to determine the efficiency loss caused by self-corrosion is believed to have relatively high accuracy.

The measured hydrogen evolution rate (P_H) of different Mg anodes are listed in Table 2. The corresponding weight loss rate (P_w) can be calculated with the conversion: P_w (mg cm^{-2} h^{-1}) = 0.994 P_H (ml cm^{-2} h^{-1}), as the working condition is nearly 25 ℃ at a pressure of 1 atm [56]. Therefore, the efficiency loss due to self-corrosion can be calculated using the following formula:

$$\eta_{sc} = \frac{W_{self-corrosion}}{W} \times 100\% = \frac{P_W \times t}{W} \times 100\% = \frac{0.994 P_H \times t}{W} \times 100\% \quad (5)$$

Where t (h) is the duration time of discharge. η_{ce} is then calculated using equation (4).

The determined efficiency loss caused by CE, η_{ce}, via this proposed approach is shown in Fig. 5. The results indicate that E21, WE43, AM50 and ZE41 anodes all exhibit high η_{ce}, especially at low current density. HP Mg and AZ31 anodes show relatively low η_{ce} and the efficiency loss is below 10% at current density of 10 mA cm^{-2}. This offers a plausible explanation for the relatively high anodic efficiency of AZ31 in spite of its fast self-corrosion rate during discharge compared to other anodes, such as E21. It is remarkable that an apparent decreasing tendency of the efficiency loss from low current density to high current density is found for all the evaluated Mg anodes, except ZE41 and AM50 at 5 mA cm^{-2}. Nevertheless, E21, WE43, AM50 and ZE41 alloys still have efficiency loss around 20-30% originated from CE. Definitely, the high η_{ce} of E21 and WE43 alloys leads to their low anodic efficiency even though they show relatively low self-corrosion rate during discharge. For instance, efficiency loss of WE43 caused by CE is 43.8% at 1mA cm^{-2}, much higher than that resulted from self-corrosion, 23.3%. ZE41 suffers the highest efficiency loss caused by CE as well as by self-corrosion, leading to the lowest anode utilization efficiency at all current densities. Generally, higher applied current density leads to more anode dissolution forced by faradic process and increased total weight loss of anode. Therefore, the proportion of weight loss caused by chunk effect in total weight loss decreases, leading to lower efficiency loss by chunk effect. However, in some cases, with increased current density, the formation of chunk effect may also be promoted, resulting in more weight loss by chunk effect. The efficiency loss due to chunk effect in this case would possibly increase even under slightly enhanced current density, the same situation for ZE41 and AM50 at 5 mA cm^{-2}. The results presented here indicate that the formation of chunk effect closely relates to the applied current density and Mg alloy category, including the microstructure and alloying elements.

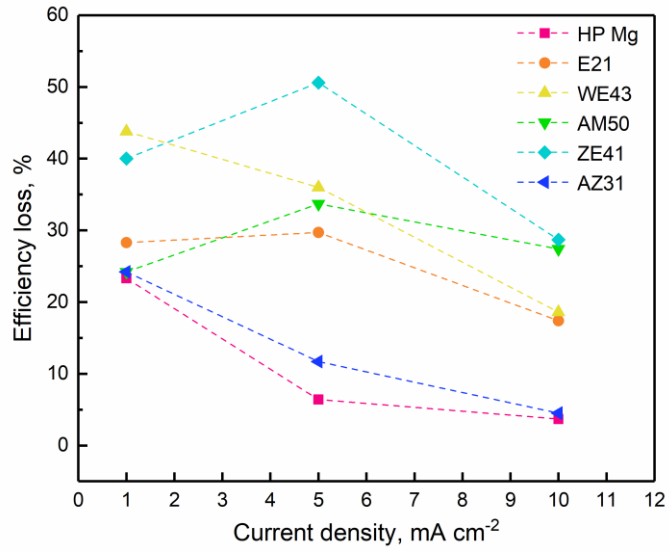

Fig. 5. Calculated efficiency loss caused by "chunk effect" for various Mg anodes at different current densities in 3.5 wt.% NaCl solution (1 mA cm^{-2} for 16 hours, 5 and 10 mA cm^{-2} for 8 hours).

The morphologies of cross section after discharge at 5 mA cm^{-2} for 8 hours are presented in Fig. 6, as a supportive evidence for the calculation results concerning efficiency loss by CE. For E21, WE43, AM50 and ZE41 alloys, the cross section indicates severe CE, appearing as large amounts of undissolved metallic portions in the discharge products layer. These separated portions are undissolved Mg matrix or second phases as demonstrated by the EDS element mapping presented in Fig. 7. Note that the elemental mapping is performed on selected areas in the cross section of E21 and WE43 anodes after discharge as shown in Fig. 6. Only the mapping results of main elements are presented here. By contrast, HP Mg and AZ31 anodes exhibit more homogeneous dissolution and corresponding discharge product layer with few separated parts, indicating only slight chunk effect. From Fig. 6 and Fig. 7, it is clear that CE appears in two forms, i.e., the separated second phases attributed to the preferential dissolution of Mg matrix around these phases (e.g., in E21) and the undermined Mg grains after the detachment of second phases surrounding this matrix (like in WE43, AM50 and ZE41). The formation of CE closely depends on the microstructure of Mg anodes, especially the constitution, quantity and distribution of the second phases. Additionally, 3D reconstruction of the surface topographies of these Mg anodes after discharge at 1 mA cm^{-2} for 16

hours are also shown in Fig. 8. It should be noted that HP Mg suffers from relatively uniform dissolution for most working surface; however, some individual grains show severe localized dissolution (see Fig. S5(a)) possibly because of special crystal orientation [57-59]. Topography of this non-uniform area is displayed here. Apparently, HP Mg, WE43 and AM50 show some large cavities on the surface after discharge. These cavities, most probably left by detachment of chunks, are the manifestation of severe CE regarding WE43 and AM50 anodes. Meanwhile, this could also be the reason that HP Mg exhibits around 20% efficiency loss by CE when discharge at 1 mA cm^{-2}. By contrast, E21, ZE41 and AZ31 alloys show relatively flat surface morphologies macroscopically. Nevertheless, separate chunks of magnesium matrix are clearly separated by dissolved second phase in case of ZE 41 alloy as seen from the SEM image under high magnification (see Fig. S5(b)). Consequently, it is noticeable that the possible occurrence of CE, especially as the form of matrix undermining, can be examined by surface morphology after discharge, but should be determined both macroscopically and microscopically.

All the experimental results mentioned here indicate that CE, namely the detachment of undissolved Mg matrix and second phases, has great influence on the efficiency of Mg anodes. In some cases, the effect of CE could exceed the impact of self-corrosion of Mg substrate, leading to low anode utilization efficiency for the Mg anodes characterized by low self-corrosion rate during the discharge. Since the presence of CE depends tightly on the chemical composition and microstructure of Mg anodes, the finding in this work demonstrates another decisive factor for the development of novel Mg anodes apart from the commonly considered self-corrosion resistance. No doubt, alloying is still an important approach to improve the self-corrosion and discharge properties of Mg anodes. However, the influence on anode utilization efficiency resulted from second-phase-relevant CE need to be elaborately considered. In order to minimize the efficiency loss caused by CE, Mg anodes with small fraction of second phase as well as discontinued distribution are requested.

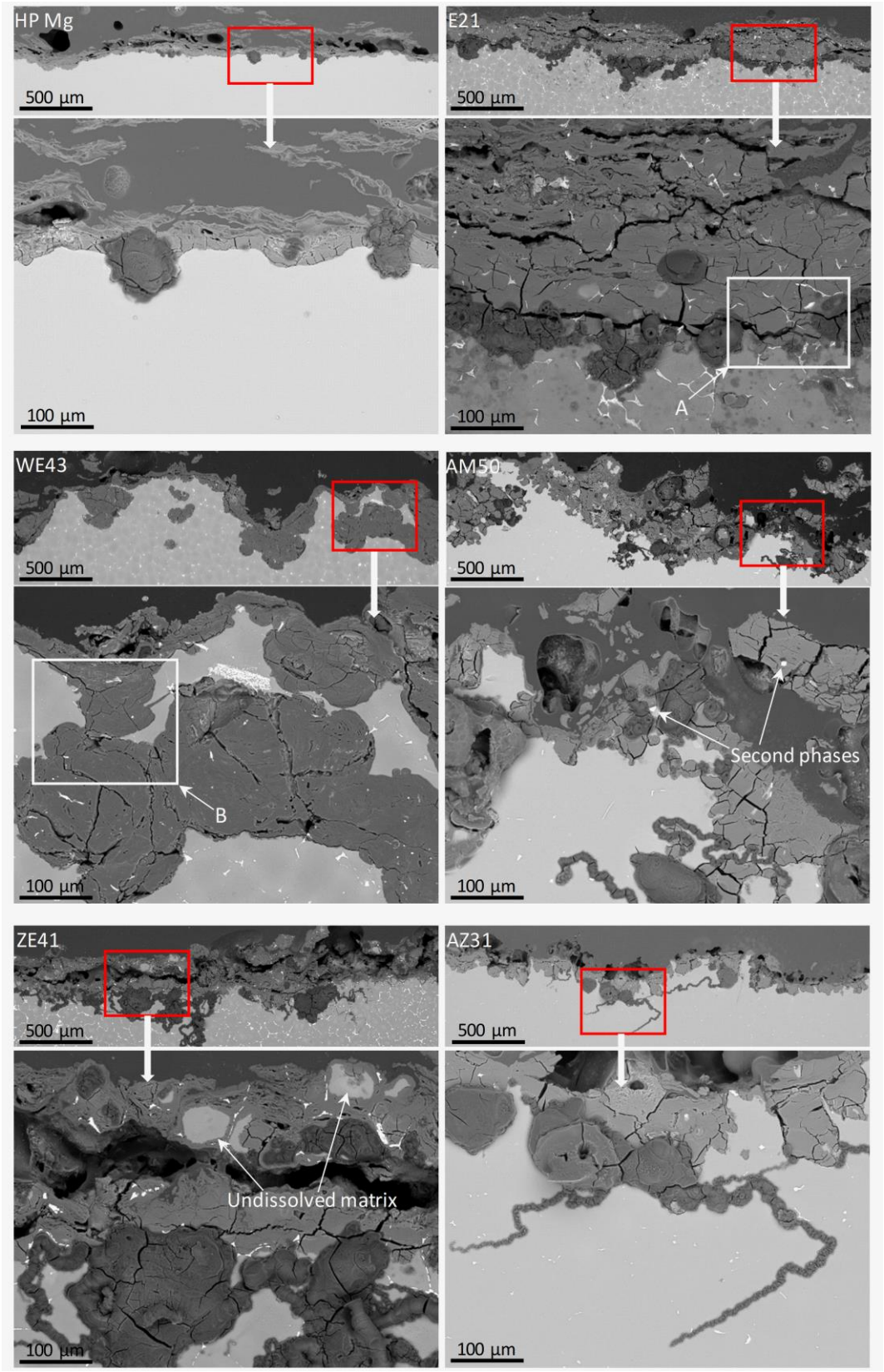

Fig. 6. Morphologies of the cross section of different Mg anodes after discharge at 5 mA cm^{-2} for 8 hours in 3.5 wt.% NaCl solution. The top layer in each cross section is an epoxy layer followed by a discharge products layer and Mg matrix.

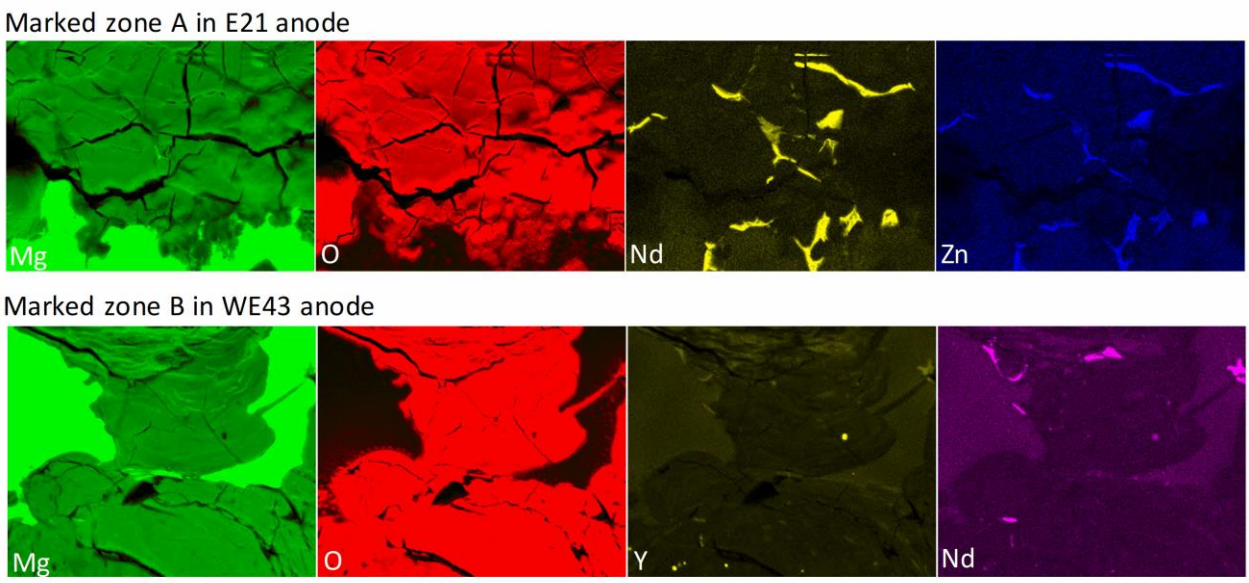

Fig. 7. Corresponding EDS mapping for the marked zone A and B respectively in the cross section of E21 and WE43 anodes after discharge as presented in Fig. 6.

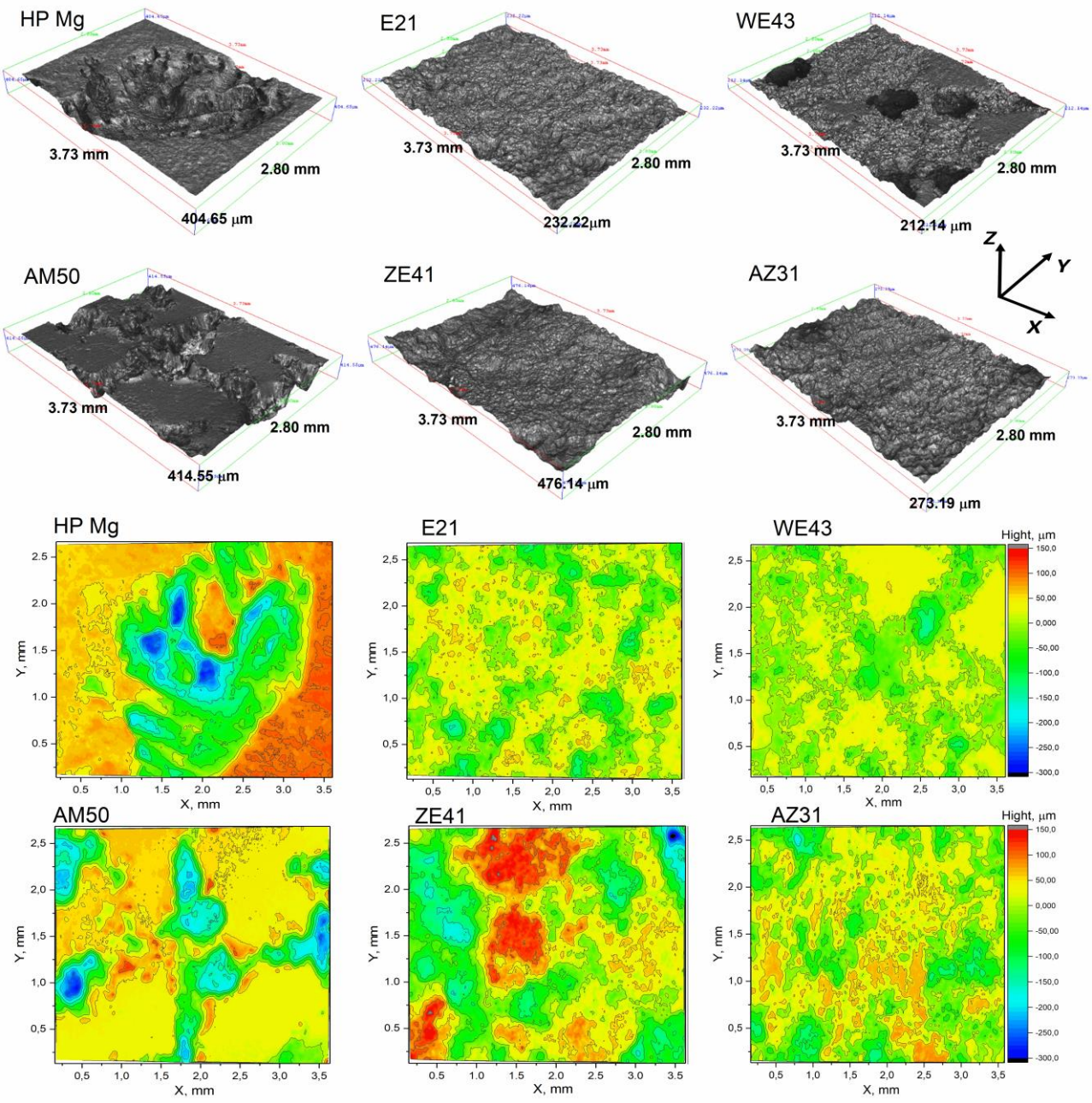

Fig. 8. 3D reconstruction indicating the topography of different Mg anodes after discharge at 1 mA cm^{-2} for 16 hours in unbuffered 3.5 wt.% NaCl solution and removal of discharge products. Corresponding depth profiles are also presented.

4. Conclusions

Discharge tests in 3.5 wt.% NaCl solution were performed on HP Mg and five Mg alloys at current densities of 1, 5 and 10 mA cm^{-2} to evaluate their utilization efficiency when served as

anodes for primary aqueous batteries under relatively small load. Corrosion resistance and self-corrosion rate at OCP of these Mg anodes are measured as well as their real-time self-corrosion rate during discharge under different current densities. The efficiency loss caused by self-corrosion of anode substrate and by detachment of undissolved metallic pieces, namely "chunk effect", is determined via a newly proposed approach. The impact of self-corrosion, at OCP and under polarization, and "chunk effect" on anodic efficiency of Mg anodes is evaluated. The following can be concluded:

(1) Self-corrosion rate determined at OCP cannot be utilized to estimate the utilization efficiency of Mg anodes during discharge. This is because the real-time self-corrosion depends on the applied discharge current density.

(2) Real-time self-corrosion rate of Mg anodes increases linearly with increase of applied discharge current density. The alloy composition and microstructure pre-determines how steeply the rate of self-corrosion increases with increase of applied discharge current density.

(3) "Chunk effect" can also cause large efficiency loss to Mg anodes, up to 50% as was shown in this work. Generally, the efficiency loss resulted from "chunk effect" is reduced with increase of current density (by 10 to 25% when discharge current increases from 1 to 10 mA cm^{-2}).

(4) In some cases, anodic efficiency loss due to "chunk effect" exceeds that caused by self-corrosion of anode, especially at low current density, being the decisive factor for the efficiency of Mg anodes.

Acknowledgement

The authors wish to acknowledge the technical support from Mr. Ulrich Burmester, Mr. Volker Heitmann and Mr. Gert Wiese regarding sample preparation and SEM operation. Additionally, M. Deng and L. Wang are grateful for the support from China Scholarship Council concerning the award of fellowship No. 201606370031 and No. 201706370183. D. Snihirova acknowledges

Humboldt foundation for Postdoctoral grant and SeaMag project for financial support (MarTera ERA-NET cofund).

References

[1] R. Renuka, AgCl and Ag2S as additives to CuI in Mg-CuI seawater activated batteries, J. Appl. Electrochem. , 27 (1997) 1394-1397. https://doi.org/10.1023/A:1018481314511.

[2] F. Cheng, J. Chen, Metal-air batteries: from oxygen reduction electrochemistry to cathode catalysts, Chem. Soc. Rev. , 41 (2012) 2172-2192. https://doi.org/10.1039/c1cs15228a.

[3] N.G. Wang, R.C. WANG, C.Q. Peng, C.W. Hu, Y. Feng, B. Peng, Research progress of magnesium anodes and their applications in chemical power sources, Transactions of Nonferrous Metals Society of China, 24 (2014) 2427-2439. https://doi.org/10.1016/S1003-6326(14)63367-7.

[4] T. Zhang, Z. Tao, J. Chen, Magnesium–air batteries: from principle to application, Mater. Horiz., 1 (2014) 196-206. https://doi.org/10.1039/c3mh00059a.

[5] R.R. Bessette, M.G. Medeiros, C.J. Patrissi, C.M. Deschenes, C.N. LaFratta, Development and characterization of a novel carbon fiber based cathode for semi-fuel cell applications, J. Power Sources 96 (2001) 240-244. https://doi.org/10.1016/S0378-7753(01)00492-X.

[6] W. Yang, S. Yang, W. Sun, G. Sun, Q. Xin, Nanostructured palladium-silver coated nickel foam cathode for magnesium–hydrogen peroxide fuel cells, Electrochim. Acta 52 (2006) 9-14. https://doi.org/10.1016/j.electacta.2006.03.066.

[7] W. Yang, S. Yang, J. Guo, G. Sun, Q. Xin, Comparison of CNF and XC-72 carbon supported palladium electrocatalysts for magnesium air fuel cell, Carbon, 45 (2007) 397-401. https://doi.org/10.1016/j.carbon.2006.09.003.

[8] C.J. Patrissi, R.R. Bessette, Y.K. Kin, C.R. Schumacher, Fabrication and Rate Performance of a Microfiber Cathode in a Mg-H_2O_2 flowing electrolyte semi-fuel cell, J. Electrochem. Soc. , 155 (2008) B558-B562. https://doi.org/10.1149/1.2901043.

[9] Z. Li, J. Yang, G. Xu, S. Wang, Non-precious cathode electrocatalyst for magnesium air fuel cells: Activity and durability of iron-polyphthalocyanine absorbed on carbon black, J. Power Sources 242 (2013) 157-165. https://doi.org/10.1016/j.jpowsour.2013.05.082.

[10] C. Shu, E. Wang, L. Jiang, G. Sun, High performance cathode based on carbon fiber felt for magnesium-air fuel cells, Int. J. Hydrogen Energy 38 (2013) 5885-5893. https://doi.org/10.1016/j.ijhydene.2013.02.093.

[11] T.R. Thomaz, C.R. Weber, T. Pelegrini, L.F.P. Dick, G. Knörnschild, The negative difference effect of magnesium and of the AZ91 alloy in chloride and stannate-containing solutions, Corros. Sci. , 52 (2010) 2235-2243. https://doi.org/10.1016/j.corsci.2010.03.010.

[12] M. Esmaily, J.E. Svensson, S. Fajardo, N. Birbilis, G.S. Frankel, S. Virtanen, R. Arrabal, S. Thomas, L.G. Johansson, Fundamentals and advances in magnesium alloy corrosion, Prog. Mater Sci. , 89 (2017) 92-193. https://doi.org/10.1016/j.pmatsci.2017.04.011.

[13] G.L. Song, A. Atrens, Corrosion Mechanisms of magnesium, Advanced Enginnering Materials, 1 (1999) 11-33. https://doi.org/10.1002/(SICI)1527-2648(199909)1:1<11::AID-ADEM11>3.0.CO;2-N.

[14] M. Deng, D. Höche, S.V. Lamaka, D. Snihirova, M.L. Zheludkevich, Mg-Ca binary alloys as anodes for primary Mg-air batteries, J. Power Sources 396 (2018) 109-118. https://doi.org/10.1016/j.jpowsour.2018.05.090.

[15] X. Li, H. Lu, S. Yuan, J. Bai, J. Wang, Y. Cao, Q. Hong, Performance of Mg–9Al–1In Alloy as Anodes for Mg-Air Batteries in 3.5 wt% NaCl Solutions, J. Electrochem. Soc. , 164 (2017) A3131-A3137. https://doi.org/10.1149/2.0971713jes.

[16] X. Liu, S. Liu, J. Xue, Discharge performance of the magnesium anodes with different phase constitutions for Mg-air batteries, J. Power Sources 396 (2018) 667-674. https://doi.org/10.1016/j.jpowsour.2018.06.085.

[17] Y. Ma, N. Li, D. Li, M. Zhang, X. Huang, Performance of Mg–14Li–1Al–0.1Ce as anode for Mg-air battery, J. Power Sources 196 (2011) 2346-2350. https://doi.org/10.1016/j.jpowsour.2010.07.097.

[18] D. Hoche, S.V. Lamaka, B. Vaghefinazari, T. Braun, R.P. Petrauskas, M. Fichtner, M.L. Zheludkevich, Performance boost for primary magnesium cells using iron complexing agents as electrolyte additives, Sci Rep, 8 (2018) 7578. https://doi.org/10.1038/s41598-018-25789-8.

[19] M.A. Deyab, Decyl glucoside as a corrosion inhibitor for magnesium–air battery, J. Power Sources 325 (2016) 98-103. https://doi.org/10.1016/j.jpowsour.2016.06.006.

[20] Y. Li, J. Ma, G. Wang, F. Ren, Y. Zhu, Y. Song, Investigation of Sodium Phosphate and Sodium Dodecylbenzenesulfunate as Electrolyte Additives for AZ91 Magnesium-Air Battery, J. Electrochem. Soc. , 165 (2018) A1713-A1717. https://doi.org/10.1149/2.0581809jes.

[21] M.M. Dinesh, K. Saminathan, M. Selvam, S.R. Srither, V. Rajendran, Water soluble graphene as electrolyte additive in magnesium-air battery system, J. Power Sources 276 (2015) 32-38. https://doi.org/10.1016/j.jpowsour.2014.11.079.

[22] S.V. Lamaka, B. Vaghefinazari, D. Mei, R.P. Petrauskas, D. Höche, M.L. Zheludkevich, Comprehensive screening of Mg corrosion inhibitors, Corros. Sci. , 128 (2017) 224-240. https://doi.org/10.1016/j.corsci.2017.07.011.

[23] H. Xiong, K. Yu, X. Yin, Y. Dai, Y. Yan, H. Zhu, Effects of microstructure on the electrochemical discharge behavior of Mg-6wt%Al-1wt%Sn alloy as anode for Mg-air primary battery, J. Alloys Compd. , 708 (2017) 652-661. https://doi.org/10.1016/j.jallcom.2016.12.172.

[24] N. Wang, R. Wang, Y. Feng, W. Xiong, J. Zhang, M. Deng, Discharge and corrosion behaviour of Mg-Li-Al-Ce-Y-Zn alloy as the anode for Mg-air battery, Corros. Sci. , 112 (2016) 13-24. https://doi.org/10.1016/j.corsci.2016.07.002.

[25] Y. Feng, W. Xiong, J. Zhang, R. Wang, N. Wang, Electrochemical discharge performance of the Mg–Al–Pb–Ce–Y alloy as the anode for Mg–air batteries, Journal of Materials Chemistry A, 4 (2016) 8658-8668. https://doi.org/10.1039/c6ta02574a.

[26] M. Yuasa, X. Huang, K. Suzuki, M. Mabuchi, Y. Chino, Discharge properties of Mg–Al–Mn–Ca and Mg–Al–Mn alloys as anode materials for primary magnesium–air batteries, J. Power Sources 297 (2015) 449-456. https://doi.org/10.1016/j.jpowsour.2015.08.042.

[27] S. Yuan, H. Lu, Z. Sun, L. Fan, X. Zhu, W. Zhang, Electrochemical Performance of Mg-3Al Modified with Ga, In and Sn as Anodes for Mg-Air Battery, J. Electrochem. Soc. , 163 (2016) A1181-A1187. https://doi.org/10.1149/2.0371607jes.

[28] N. Wang, R. Wang, C. Peng, B. Peng, Y. Feng, C. Hu, Discharge behaviour of Mg-Al-Pb and Mg-Al-Pb-In alloys as anodes for Mg-air battery, Electrochim. Acta 149 (2014) 193-205. https://doi.org/10.1016/j.electacta.2014.10.053.

[29] M. Yuasa, X. Huang, K. Suzuki, M. Mabuchi, Y. Chino, Effects of Microstructure on Discharge Behavior of AZ91 Alloy as Anode for Mg-Air Battery, Materials Transaction, 55 (2014) 1202-1207. https://doi.org/10.2320/matertrans.MC201403.

[30] G.A. Marsh, E. Schaschl, The Difference Effect and the Chunk Effect, J. Electrochem. Soc. , 107 (1960) 960-965. https://doi.org/10.1149/1.2427579

[31] M.E. Straumanis, B.K. Bhatia, Disintegration of Magnesium While Dissolving Anodically in Neutral and Acidic solutions, J. Electrochem. Soc. , 110 (1963) 357-360. https://doi.org/10.1149/1.2425763.

[32] M. Andrei, F.d. Gabriele, P.L. Bonora, D. Scantlebury, Corrosion behaviour of magnesium sacrificial anodes in tap water, Mater. Corros. , 54 (2003) 5-11. https://doi.org/10.1002/maco.200390010.

[33] P. Jiang, C. Blawert, R. Hou, N. Scharnagl, J. Bohlen, M.L. Zheludkevich, Microstructural influence on corrosion behavior of MgZnGe alloy in NaCl solution, J. Alloys Compd. , 783 (2019) 179-192. https://doi.org/10.1016/j.jallcom.2018.12.296.

[34] A. Samaniego, N. Birbilis, X. Xia, G.S. Frankel, Hydrogen Evolution During Anodic Polarization of Mg Alloyed with Li, Ca, or Fe, Corrosion, 71 (2015) 224-233. https://doi.org/10.5006/1367.

[35] P.-W. Chu, E. Le Mire, E.A. Marquis, Microstructure of localized corrosion front on Mg alloys and the relationship with hydrogen evolution, Corros. Sci. , 128 (2017) 253-264. https://doi.org/10.1016/j.corsci.2017.09.022.

[36] D. Cao, L. Wu, Y. Sun, G. Wang, Y. Lv, Electrochemical behavior of Mg–Li, Mg–Li–Al and Mg–Li–Al–Ce in sodium chloride solution, J. Power Sources 177 (2008) 624-630. https://doi.org/10.1016/j.jpowsour.2007.11.037.

[37] M.C. Lin, C.Y. Tsai, J.Y. Uan, Electrochemical behaviour and corrosion performance of Mg–Li–Al–Zn anodes with high Al composition, Corros. Sci. , 51 (2009) 2463-2472. https://doi.org/10.1016/j.corsci.2009.06.036.

[38] R. Udhayan, N. Muniyandi, P.B. mathur, Studies on magnesium and its alloys in battery electrolytes, British Corroison Journal, 27 (1992) 68-71. https://doi.org/10.1179/000705992798268927.

[39] Y.-Z. Lv, Y.-Z. Jin, Z.-B. Wang, M. Liu, Y.-F. Li, L. Wang, D.-X. Cao, The electrochemical behaviors of the Mg-7.5Li-3.5Al and Mg-7.5Li-3.5Al-1Y electrodes in sodium chloride solution, Ionics, 21 (2014) 429-435. https://doi.org/10.1007/s11581-014-1187-z.

[40] D. Cao, L. Wu, G. Wang, Y. Lv, Electrochemical oxidation behavior of Mg–Li–Al–Ce–Zn and Mg–Li–Al–Ce–Zn–Mn in sodium chloride solution, J. Power Sources 183 (2008) 799-804. https://doi.org/10.1016/j.jpowsour.2008.06.005.

[41] J. Li, B. Zhang, Q. Wei, N. Wang, B. Hou, Electrochemical behavior of Mg-Al-Zn-In alloy as anode materials in 3.5 wt.% NaCl solution, Electrochim. Acta 238 (2017) 156-167. https://doi.org/10.1016/j.electacta.2017.03.119.

[42] D. Cao, X. Cao, G. Wang, L. Wu, Z. Li, Electrochemical discharge performance of Mg-Li based alloys in NaCl solution, J. Solid State Electrochem. , 14 (2009) 851-855. https://doi.org/10.1007/s10008-009-0865-7.

[43] Y. Shi, C. Peng, Y. Feng, R. Wang, N. Wang, Microstructure and electrochemical corrosion behavior of extruded Mg–Al–Pb–La alloy as anode for seawater-activated battery, Materials & Design, 124 (2017) 24-33. https://doi.org/10.1016/j.matdes.2017.03.058.

[44] N. Wang, R. Wang, C. Peng, Y. Feng, Enhancement of the discharge performance of AP65 magnesium alloy anodes by hot extrusion, Corros. Sci. , 81 (2014) 85-95. https://doi.org/10.1016/j.corsci.2013.12.005.

[45] G.S. Frankel, A. Samaniego, N. Birbilis, Evolution of hydrogen at dissolving magnesium surfaces, Corros. Sci. , 70 (2013) 104-111. https://doi.org/10.1016/j.corsci.2013.01.017.

[46] L.Q. Wang, R.C. Wang, Y. Feng, M. Deng, N.G. Wang, Effect of Al and Pb Contents on the Corrosion Electrochemical Properties and Activation of Mg-Al-Pb Alloy Anode, J. Electrochem. Soc. , 164 (2017) A438-A446. https://doi.org/10.1149/2.1211702jes.

[47] A. Pardo, M.C. Merino, A.E. Coy, F. Viejo, R. Arrabal, S. Feliú, Influence of microstructure and composition on the corrosion behaviour of Mg/Al alloys in chloride media, Electrochim. Acta 53 (2008) 7890-7902. https://doi.org/10.1016/j.electacta.2008.06.001.

[48] R. Arrabal, A. Pardo, M.C. Merino, M. Mohedano, P. Casajús, K. Paucar, G. Garcés, Effect of Nd on the corrosion behaviour of AM50 and AZ91D magnesium alloys in 3.5 wt.% NaCl solution, Corros. Sci. , 55 (2012) 301-312. https://doi.org/10.1016/j.corsci.2011.10.033.

[49] W. Liu, F. Cao, L. Chang, Z. Zhang, J. Zhang, Effect of rare earth element Ce and La on corrosion behavior of AM60 magnesium alloy, Corros. Sci. , 51 (2009) 1334-1343. https://doi.org/10.1016/j.corsci.2009.03.018.

[50] S. Fajardo, G.S. Frankel, Effect of impurities on the enhanced catalytic activity for hydrogen evolution in high purity magnesium, Electrochim. Acta 165 (2015) 255-267. https://doi.org/10.1016/j.electacta.2015.03.021.

[51] S. Fajardo, G.S. Frankel, Gravimetric Method for Hydrogen Evolution Measurements on Dissolving Magnesium, J. Electrochem. Soc. , 162 (2015) C693-C701. https://doi.org/10.1149/2.0241514jes.

[52] E.L. Silva, S.V. Lamaka, D. Mei, M.L. Zheludkevich, The Reduction of Dissolved Oxygen During Magnesium Corrosion, ChemistryOpen, 7 (2018) 664-668. https://doi.org/10.1002/open.201800076.

[53] D. Mei, S.V. Lamaka, J. Gonzalez, F. Feyerabend, R.W. Römer, M.L. Zheludkevich, The role of individual components of simulated body fluid on the corrosion behavior of commercially pure Mg, Corros. Sci. , 147 (2018) 81-93. https://doi.org/10.1016/j.corsci.2018.11.011.

[54] S.V. Lamaka, J. Gonzalez, D. Mei, F. Feyerabend, R. Willumeit-Römer, M.L. Zheludkevich, Local pH and Its Evolution Near Mg Alloy Surfaces Exposed to Simulated Body Fluids, Advanced Materials Interfaces, 5 (2018) 1800169. https://doi.org/10.1002/admi.201800169.

[55] J. Izquierdo, B.M. Fernández-Pérez, D. Filotás, Z. Őri, A. Kiss, R.T. Martín-Gómez, L. Nagy, G. Nagy, R.M. Souto, Imaging of Concentration Distributions and Hydrogen Evolution on Corroding Magnesium Exposed to Aqueous Environments Using Scanning Electrochemical Microscopy, Electroanalysis, 28 (2016) 2354-2366. https://doi.org/10.1002/elan.201600265.

[56] Z. Qiao, Z. Shi, N. Hort, N.I. Zainal Abidin, A. Atrens, Corrosion behaviour of a nominally high purity Mg ingot produced by permanent mould direct chill casting, Corros. Sci. , 61 (2012) 185-207. https://doi.org/10.1016/j.corsci.2012.04.030.

[57] G.-L. Song, Z. Xu, Crystal orientation and electrochemical corrosion of polycrystalline Mg, Corros. Sci. , 63 (2012) 100-112. https://doi.org/10.1016/j.corsci.2012.05.019.

[58] M. Liu, D. Qiu, M.-C. Zhao, G. Song, A. Atrens, The effect of crystallographic orientation on the active corrosion of pure magnesium, Scr. Mater. , 58 (2008) 421-424. https://doi.org/10.1016/j.scriptamat.2007.10.027.

[59] L.G. Bland, K. Gusieva, J.R. Scully, Effect of Crystallographic Orientation on the Corrosion of Magnesium: Comparison of Film Forming and Bare Crystal Facets using Electrochemical Impedance and Raman Spectroscopy, Electrochim. Acta 227 (2017) 136-151. https://doi.org/10.1016/j.electacta.2016.12.107.